科学通报 2025 年 第 70 卷 第 26 期: 4525 ~ 4537
离子液体在能源、环境和材料中的应用专题 论 文
《中国科学》杂志社 SCIENCE CHINA PRESS

季铵盐离子液体对氨基酸铜催化CO_2环加成反应的协同机制

肖自胜, 刘思怡, 宋涂暄, 李丹, 兰支利, 肖毅*, 谭蓉*, 尹笃林

石化新材料与资源精细利用国家地方联合工程实验室, 湖南师范大学化学化工学院, 长沙 410081
* 联系人, E-mail: xiaoyi@hunnu.edu.cn; yiyangtanrong@126.com

2025-04-25 收稿, 2025-06-12 修回, 2025-06-30 接受, 2025-07-31 网络版发表
国家自然科学基金(22178093, 22278122)和湖南省科技规划项目(2018TP1017)资助

摘要 四丁基卤化铵(TBAX)离子液体与氨基酸铜配合物(CuAAs)在CO_2与环氧化物的环加成反应中表现出理想的协同催化活性. 采用四种天然氨基酸(甘氨酸、丙氨酸、异亮氨酸和苯丙氨酸)和铜(Ⅱ)制备了相应的配合物并对其进行结构与形貌表征. 以CuAAs为主催化剂, TBAX为助催化剂, 研究了CuAAs/TBAX在CO_2与氧化苯乙烯环加成反应中的协同催化性能. 实验结果表明, 在CuAAs/TBAX协同催化体系中, 环碳酸酯的收率可达71.3%~85.1%. 基于密度泛函理论(DFT)计算, 探讨了CuAAs和TBAX在CO_2环加成反应中的协同作用机制. DFT计算表明, 氧化苯乙烯的开环过程是反应的决速步骤, 甘氨酸铜/四丁基溴化铵协同催化体系具有较低的过渡态能垒(+19.4 kcal/mol). 在氧化苯乙烯开环、CO_2插入和碳酸酯闭环过程中, CuAAs和TBAX的协同作用是不可或缺的, TBAX的协同作用可能主要影响氧化苯乙烯的开环和碳酸酯的闭环过程, CuAAs则可能更有利于CO_2的活化. 利用CuAAs与TBAX的协同作用是构建系列简单可行的CO_2环加成催化体系的重要策略之一, 这为CO_2化学转化绿色路径的设计提供了实验和理论支持.

关键词 氨基酸-Cu配合物, 季铵盐离子液体, CO_2环加成, 协同催化反应, 密度泛函理论(DFT)

CO_2的大量排放是全球气候变暖的主要原因之一[1,2]. 为了实现“碳达峰”和“碳中和”的“双碳”战略目标, 各国政府纷纷采取措施以减少CO_2的排放[3,4]. 相关研究人员对CO_2的捕集、储存和利用进行了广泛的研究, 特别是利用CO_2合成高附加值化学品的策略更是引起了相关研究人员的极大兴趣[5,6]. 由CO_2和环氧化物环加成反应生成的环碳酸酯是一大类用途广泛的化学物质, 已被广泛用做溶剂、合成聚碳酸酯的前驱体、表面活性剂和增塑剂生产的中间体[7,8]. 大量的均相或多相催化体系被开发以用于CO_2的环加成[9~11], 包括氨基酸离子液体[12~14]、过渡金属有机框架材料(MOFs)[15~17]等. 氨基酸铜配合物(CuAAs)作为天然的生物相容性材料而受到研究者的青睐[18], 据报道, 氨基酸的氨基及羧基对CO_2的活化具有催化作用[19,20].

尽管CuAAs在CO_2环加成反应中展现巨大的潜力[21,22], 但仅用CuAAs很难达到理想的催化效果[23]. 研究表明, 季铵盐类离子液体(TBAX)能促进CO_2的环加成反应[24~28], 但对CuAAs和TBAX的协同催化作用机理不明确[29]. 本文采用简单的方法合成了4种CuAAs (甘氨酸铜(CuGly)、丙氨酸铜(CuAla)、异亮氨酸铜(CuIle)和苯丙氨酸铜(CuPhe)), 并对其结构和形貌进行了表征, 研究了在温和条件下(80℃, CO_2压力1 atm), 以CuAAs为主催化剂、TBAX为助催化剂在CO_2与氧化苯乙烯(StO)环加成反应中的协同催化性能. 采用密度

引用格式: 肖自胜, 刘思怡, 宋涂暄, 等. 季铵盐离子液体对氨基酸铜催化CO_2环加成反应的协同机制. 科学通报, 2025, 70: 4525–4537
Xiao Z, Liu S, Song T, et al. Synergistic mechanism of quaternary ammonium salt ionic liquid in CO_2 cycloaddition reaction catalyzed by amino acid copper (in Chinese). Chin Sci Bull, 2025, 70: 4525–4537, doi: 10.1360/CSB-2025-0589

泛函理论(density functional theory, DFT)计算方法, 模拟了四种CuAAs与四丁基溴化铵(TBAB)协同催化CO_2环加成的反应过程, 比较了CuGly和TBAX在StO开环、CO_2插入和碳酸酯闭环中的协同作用机理. 采用基于Hirshfeld独立梯度模型(Independent Gradient Model Based on Hirshfeld Partition, IGMH)的方法, 分析了CuGly/TBAB协同催化过程中分子片段之间的弱相互作用. DFT计算结果表明, StO的开环过程是反应的决速步骤, CuGly/TBAB协同催化体系具有较低的过渡态能垒(+19.4 kcal/mol). 此外, CuAAs和TBAX的协同作用在StO开环、CO_2插入和碳酸酯闭环过程中是不可或缺的, TBAX的协同作用可能主要影响StO的开环和碳酸酯的闭环过程, CuAAs则可能更有利于CO_2的活化. 该研究揭示了CuAAs/TBAX催化CO_2环加成的反应机制, 利用TBAX对CuAAs催化CO_2环加成反应的协同机制构建了系列简单可行的CO_2环加成反应策略, 为CO_2综合利用的催化剂设计提供了实验和理论支持.

1 实验

1.1 化学试剂

CO_2购自长沙曼德气体有限公司(纯度99.99%), 实验中所有原材料均未经过进一步纯化, 直接用于实验. 甘氨酸(Gly, 98%)、*L*-丙氨酸(Ala, 99%)、异亮氨酸(Ile, 99%)、苯丙氨酸(Phe, 99%)、四丁基氯化铵(TBAC)(95%)、TBAB(99%)以及四丁基碘化铵(TBAI)(99%)等均购于北京百灵威科技有限公司.

1.2 催化剂制备

根据文献[20,30~32]报道的方法制备CuAAs催化剂. 将氨基酸(1 mmol, Gly: 75 mg, Ala: 89 mg, Ile: 131 mg, Phe: 165 mg)溶于10 mL去离子水中, 然后在上述溶液中加入NaOH(1 mmol, 40 mg), 60℃下搅拌2 h. 将$Cu(NO_3)_2{\cdot}3H_2O$(0.5 mmol, 120.8 mg)溶于4 mL去离子水中, 然后将其缓慢滴入上述氨基酸溶液中, 溶液经超声处理20 min后, 移入水热反应釜, 80℃烘箱中放置30 h. 用EtOH洗涤两次, 60℃真空干燥12 h, 收集并密封样品用于表征和催化性能测试.

1.3 CO_2和StO的环加成

CO_2环加成反应在三口烧瓶(体积为10 mL)中进行, CO_2从水封装置中供应. 简单地说, 在烧瓶中加入适量的StO、CuAAs和(或)TBAX, 然后在80℃、1 atm CO_2压力下进行CO_2环加成反应[33]. 反应完成后, 用乙酸乙酯萃取反应液, 并用气相色谱仪对混合物进行定量分析, 用GC-MS、^{1}H NMR和^{13}C NMR对纯化的环碳酸酯进行表征.

1.4 催化剂表征方法

红外光谱采用KBr压片法, 使用美国Nicolet公司生产的Nicolet 370红外光谱仪采集波长范围为400~4000 cm^{-1}的吸收光谱; X射线衍射(XRD)测试以Cu靶Kα作为X射线放射源, 在荷兰PANalytical B.V.公司生产的X射线衍射仪上完成, 扫描范围为5°~50°; 样品经硝酸处理后, 使用美国Thermo Fisher公司生产的ICAP 7200型电感耦合等离子体发射光谱仪(ICP-OES)测定铜含量; X射线光电子能谱(XPS)使用美国Thermo Fisher公司生产的ESCALAB 250Xi型X射线光电子能谱仪; 使用日本JEOL公司生产的JSM-2100透射电子显微镜(TEM)进行微观形貌和结构分析; ^{1}H NMR及^{13}C NMR采用德国Bruker公司生产的Avance 500 MHz超导核磁共振波谱仪; 采用配备FID检测器的日本Shimadzu GC-2014C气相色谱仪(HP-5, 30 m × 0.32 mm × 0.25 μm)进行定量分析.

1.5 DFT理论计算

利用WB97XD泛函[34], 结合C、H、O、N原子的DEF2SVP[35]和Cu、卤素(Cl、Br、I)离子的LANL2DZ[36,37]混合基组进行几何优化和振动频率的计算, 该DFT计算方法为金属有机配合物(包括CuAAs)和催化反应的计算提供了良好的结果[38,39]. 振动频率的计算证实了该物种的稳态结构没有虚频率, 过渡态有且只有一个虚频率. 在相同的计算水平上进行本征反应坐标(intrinsic reaction coordinate, IRC)计算, 定位过渡态(transition state, TS), 确认各反应路径的有效性[40]. 初始反应系统(即催化剂加底物)的总能量设为零, 各物种的吉布斯自由能数值是吉布斯自由能修正和单点能的组合. 基于计算结果, 采用Multiwfn软件包[41]结合可视化分子动力学(Visual Molecular Dynamics, VMD)程序[42]对CuAAs配合物的表面静电势(electrostatic potential surfaces, ESP)进行研究, 采用IGMH方法分析CuGly/TBAB协同催化中分子片段之间的弱相互作用. 所有计算均在Gaussian 09程序中进行[43].

2 结果与讨论

2.1 催化剂表征

CuAAs和氨基酸的FT-IR光谱如图1所示. 在1612和3160 cm^{-1}处, ν(N-H)的强吸收带是由Gly中的羧基和氨基伸缩振动引起的(图1(a)), Gly与Cu(Ⅱ)配位后, 其ν(N-H)和ν(COO-)的吸收带发生了轻微的位移, 3160 cm^{-1}的ν(N-H)吸收峰向更高波长(3266 cm^{-1})的移动归因于氨基氮原子与Cu(Ⅱ)之间的结合, 由于Cu(Ⅱ)和羰基之间的相互作用, ν(COO-)在1612 cm^{-1}的吸收峰向低波长(1605 cm^{-1})移动. 559 cm^{-1}处的新吸收带则可归属于Cu-N(-NH_2)的伸缩振动[44]. 同样, 由Ala和CuAla在16191、3239、574 cm^{-1}处波长的变化(图1(b))、Ile和CuIle在1622、33267、571 cm^{-1}处波长的变化(图1(c))、Phe和CuPhe在1619、3249、557 cm^{-1}处波长的变化(图1(d))可知, 由于Cu和氨基酸之间的化学配位作用引起了低频振动耦合[45], FT-IR表明氨基酸配体主要采用羧基氧及氨基氮参与Cu(Ⅱ)配位[46].

CuAAs的XRD光谱如图2(a)所示. 由图可知, 10.5°、17.6°、25.7°、38.2°是CuGly的特征衍射峰(JCPDS No. 17-1814), 19.9°、29.4°、38.1°处为CuAla的特征衍射峰; 同样, 在19.2°、29.4°、38.1°处是CuIle的特征衍射峰(CCDC No. 1818079), 10.7°、16.0°、38.1°处为CuPhe的特征衍射峰(PDF# 32-1605), 这些表征结果与相关文献[20,30~32]的结论一致, 表明合成的配合物具有相应的单斜晶体结构. 利用TEM对合成的CuAAs进行了形貌表征, TEM图显示其均具有明显的片状结构(图S1), 这可能为CO_2的环加成反应提供了一个合适的空间取向.

采用XPS分析了Cu(Ⅱ)金属中心的氧化态, 由

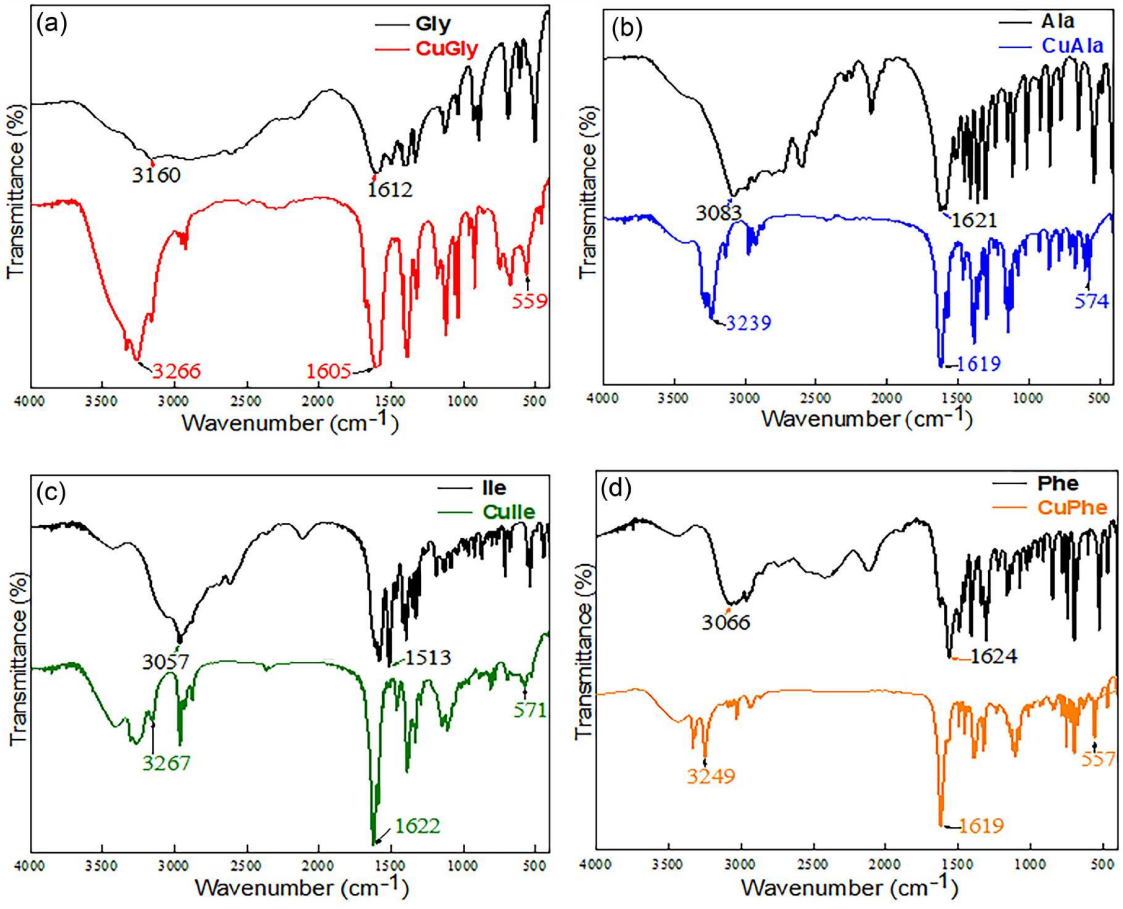

图 1 (网络版彩色)CuAAs及其对应氨基酸配体的红外光谱图. (a) Gly与CuGly; (b) Ala与CuAla; (c) Ile与CuIle; (d) Phe与CuPhe

Figure 1 (Color online) Infrared spectra of CuAAs and their corresponding amino acid ligands. (a) Gly and CuGly; (b) Ala and CuAla; (c) Ile and CuIle; (d) Phe and CuPhe

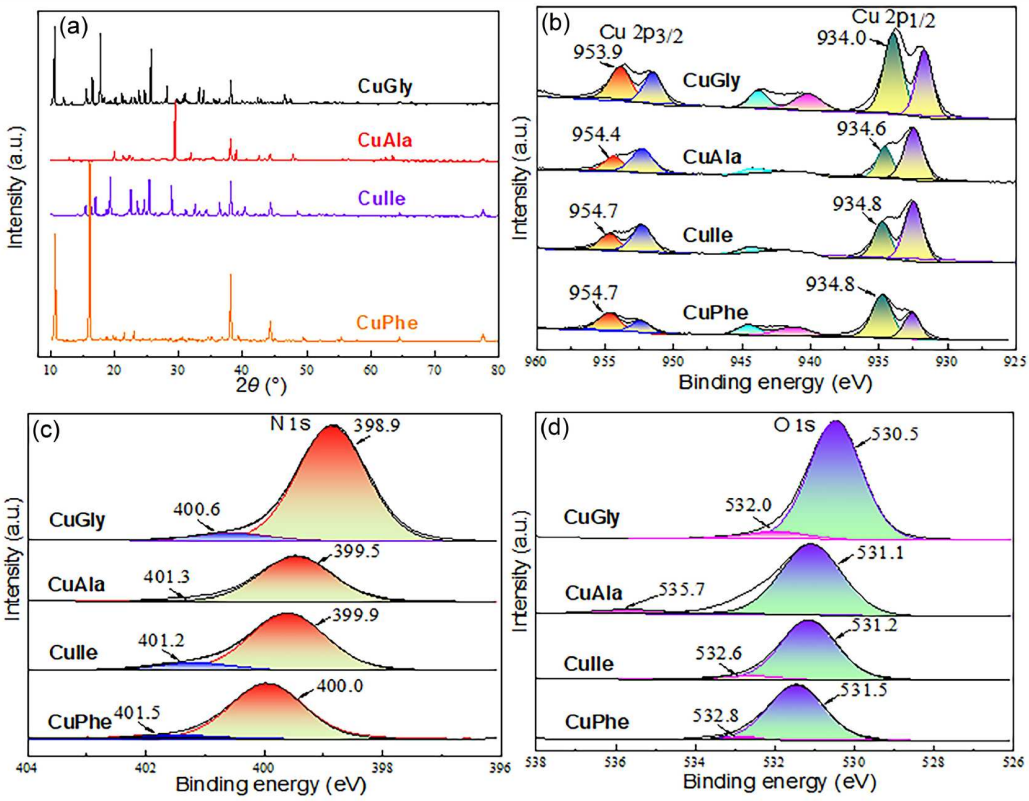

图 2 (网络版彩色)CuAAs的XRD(a)和Cu(b)、N(c)、O(d)元素的XPS精细谱图
Figure 2 (Color online) The XRD spectra (a) of CuAAs and XPS fine spectra of element Cu (b), N (c), and O (d) in CuAAs

图2(b)可知, 四种CuAAs中铜元素的Cu $2p_{1/2}$和Cu $2p_{3/2}$分别在954.7和934.4 eV附近处呈现吸收峰, 按CuGly、CuAla、CuIle和CuPhe顺序, 其对应结合能相应增加, 其中CuGly具有最小的结合能(953.9及934.0 eV). 这主要是因为氨基酸中的N、O原子与Cu活性中心配位后, 增加了Cu原子周围的电子密度, 从而使Cu原子外层电子对其内核电子的屏蔽效应增强, 导致内核电子感受到的有效核电荷减少, 结合能降低; 同样, 在相应的CuAAs中N、O元素精细谱中也存在相应的差异(图2(c), (d)). 这些差异形成的原因可能主要来自CuAAs的不同氨基酸配体中N、O原子配位能力的差异, CuGly因具有较小的配体结构更有利于与铜中心配位, 对应的CuPhe及CuIle则可能因其苯环(或多支链-CH_3)配体构筑了较大的空间位阻, 而使其具有较大的结合能(954.7及934.8 eV). CuAAs的XPS检测结果与文献[31,32]报道的数据基本一致, 确定了CuAAs配合物的形成. 此外, ICP-OES分析显示CuGly、CuAla、CuIle和CuPhe的铜元素质量分数分别为29.35%、25.83%、19.77%和16.45%, 这与相应的理论计算值(29.72%、26.27%、19.49%和16.12%)是一致的.

2.2 催化剂的电子结构

ESP分析对于研究CuAAs配合物与反应底物分子之间的静电相互作用、预测反应位点、预测分子性质等具有重要意义. 基于CuAAs分子范德华势能面的ESP能谱如图3所示. 在CuAAs的ESP表面, 红色中心对应正电荷较高的正极区域, 而电子密度较高的负极区域则用蓝色表示[47]. 氨基酸羧基(COO^-)位于静电电位更负的区域, 而氨基酸与Cu(Ⅱ)配位形成的对称纺锤形活性中心则位于静电电位更正的区域. 定量分析表明CuGly表面具有高于其他三种CuAAs的最高正静电势(+51.99 kcal/mol), 其中CuAla与CuIle差别不大, CuPhe最小(+48.17 kcal/mol). 表明CuGly的铜活性中心可能更为暴露而具备更强的氢键给体性质, 这一变化趋势与其XPS检测结果一致, 这为反应提供了更合适的协同催化位点.

2.3 催化性能测试

在CO_2与StO环加成反应中考察了不同CuAAs配合物催化剂的催化性能，实验结果如表1所示. 无催化剂的空白对照实验(表1, 序号1)表明, 催化剂对CO_2和StO环加成反应是至关重要的. 仅使用主催化剂CuGly(表1, 序号4)或主催化剂各组分(Gly及$Cu(NO_3)_2·3H_2O$)(表1, 序号2，3)也没有表现出有价值的催化活性. 仅使用TBAB时，StO的转化率为30%(表1，序号5)，而使用CuGly和TBAB协同催化，StO的转化率则可达80%(表1，序号6)，使用CuAla、CuIle及CuPhe分别与TBAB组合时，StO的转化率则在72%以上(表1，序号7~9). 在

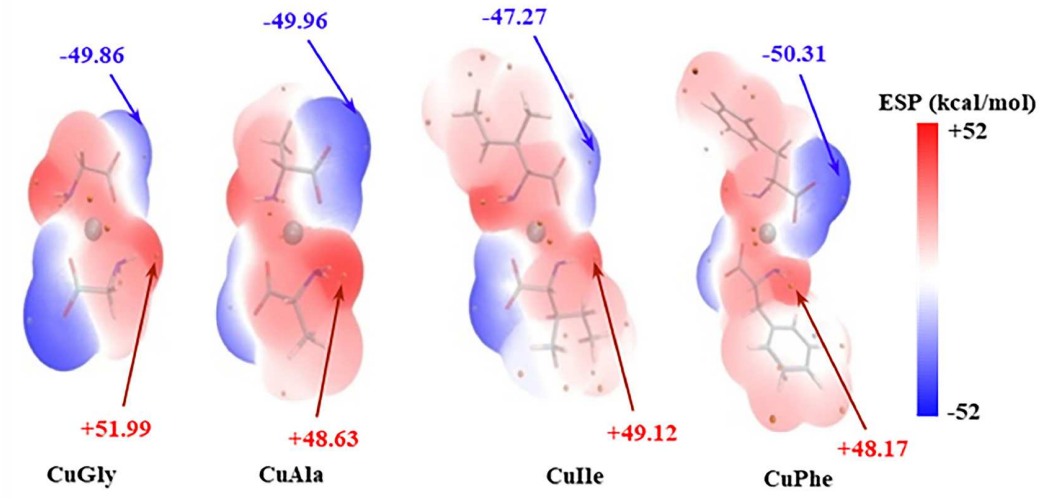

图 3 (网络版彩色)基于范德华表面分析CuAAs的ESP图
Figure 3 (Color online) ESP-mapped molecular van der Waals' surface of CuAAs

表 1 (网络版彩色)不同反应条件下CO_2与StO的环加成反应[a)]
Table 1 (Color online) Cycloaddition reaction of CO_2 and StO under different reaction conditions

序号	主催化剂	助催化剂	Sto转化率(%)	选择率(%)	收率(%)
1	无	无	< 1	/	< 1
2	Gly	无	3	99	3.0
3	$Cu(NO_3)_2·3H_2O$	无	5	99	5.0
4	CuGly	无	3	99	3.0
5	无	TBAB	30	99	29.7
6	CuGly	TBAB	80	99	79.2
7[b)]	CuAla	TBAB	75	99	74.3
8[c)]	CuIle	TBAB	73	99	72.3
9[d)]	CuPhe	TBAB	72	99	71.3
10[e)]	CuGly	TBAC	73	99	72.3
11[f)]	CuGly	TBAI	78	99	77.2
12[g)]	CuGly	TBAI	82	99	81.2
13[h)]	CuGly	TBAB	86	99	85.1

a) 反应条件: 如无特别说明, StO(120 mg, 1.0 mmol), CuGly(0.4 mol%, 5 mg), TBAB(5 mol%, 16 mg), T = 80℃, t = 18 h, CO_2 (1 atm). b) CuAla (0.4 mol%, 6 mg). c) CuIle(0.4 mol%, 8 mg). d) CuPhe(0.4 mol%, 9 mg). e) TBAC(5 mol%, 14 mg). f) TBAI(5 mol%, 18 mg). g) TBAI(5 mol%, 18 mg), t = 24 h. h) TBAB(5 mol%, 16 mg), t = 24 h

同等条件下, 延长CuGly/TBAI的催化反应时间, StO的转化率则可略有上升, 环碳酸酯收率可达81.2%(表1, 序号12), 而对比延长CuGly/TBAB的催化反应时间, StO的转化率则可达86%, 环碳酸酯收率可达85.1%(表1, 序号13). 此外, 在同等条件下, 考察了TBAB用量对CuGly/TBAB协同催化反应的影响(图S2), 表明TBAX用量对反应存在着一定的影响, 其中TBAB用量为StO用量的5 mol%(16 mg)为宜. 以上实验结果分析表明, 在CO_2环加成反应中, CuAAs和TBAB之间存在着的协同催化作用是反应得以高效进行的关键. 对比CuAAs与TBAC、TBAB和TBAI组合的协同催化实验结果(表1, 序号6, 10, 11), 发现TBAB和TBAI表现出较好的催化性能. 这表明助催化剂的基本性质对CO_2环加成反应存在较大的影响. 此外, CuGly/TBAB催化体系具有优良的稳定性, 使用5次以上其催化性能仍能得以较好保持(图S3).

2.4 CuAAs与TBAB(协同)催化机理

CuAAs/TBAB协同催化主要包括三个典型的基本反应过程, 即环氧化物开环、CO_2插入和碳酸酯闭环[48,49]. 对比研究非催化条件及仅用CuAAs(或TBAB)催化条件下的CO_2环加成机理, 有助于阐明CuAAs/TBAB催化体系在CO_2环加成中的协同催化作用[50]. 图4(a)为各反应可能中间体和TS的吉布斯自由能分布图, 图4(b)为主要对应物种的优化结构图. 在非催化条件下, CO_2与StO环加成反应理论上只需一步即可完成, 环加成反应以CO_2分子配位到StO的O原子上形成络合物Com1_1开始, 生成Com1_1的热效应为吸热+3.1 kcal/mol, 畸高的能垒(+457.3 kcal/mol)表明非催化反应无法进行. 同样, 高达+53.2 kcal/mol的能垒也表明仅由CuAla催化的反

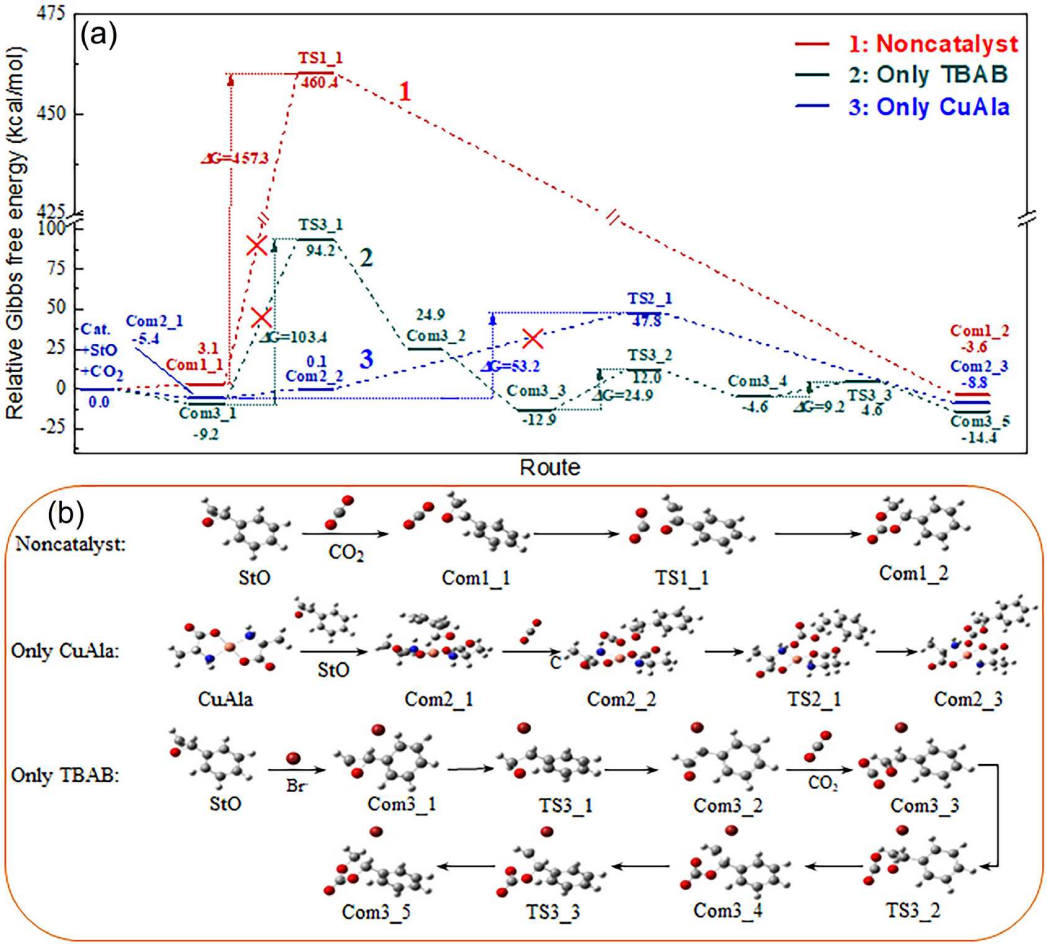

图 4 (网络版彩色)非(或非协同)催化反应的吉布斯自由能分布图(a)及优化的可能中间体和TS图(b)

Figure 4 (Color online) Gibbs free energy profiles of non- (or non-synergistic-) catalytic reactions (a) and the optimized intermediates and TS of reaction routes (b)

应难以进行. 此外, 仅使用TBAB催化StO开环的吉布斯能垒高达+103.4 kcal/mol, 这也意味着CO_2环加成需要苛刻的反应条件. 因此, 为了降低反应能垒, 采用CuAAs和TBAB的协同催化是实现温和条件下CO_2高效环加成反应颇具潜力的策略之一.

基于CuGly/TBAB在实验过程中表现出优秀的协同催化效果, 对比探讨了四种CuAAs/TBAB体系在CO_2环加成中的协同催化机理[49,50]. 图5(a)为CuAAs/TBAB反应路线的吉布斯自由能分布图, 图5(b)为CuGly/TBAB催化体系中可能的中间体和TS优化结构, CuAla、CuIle及CuPhe与TBAB协同催化体系中可能的中间体和TS优化结构见图S4. CuAAs/TBAB催化反应开始于StO的O原子配位到CuAAs的活性Cu(Ⅱ)位点上, 从而生成Cu(Ⅱ)与StO配位的中间体Com_1. Com_1中Cu(Ⅱ)的配位引起StO分子中的C−O键(C_α−O和C_β−O键)发生极化, 使其α/β-C原子对亲核试剂Br^-(TBAB)的进攻更为敏感. StO分别与CuGly, CuAla、CuIle形成Com4_1、Com5_1、Com6_1过程中对应的热效应为放热−19.0、−7.1和−5.4 kcal/mol, 表明从反应物到com_1的步骤是可以自发的. 而StO与CuPhe的配合物形成过程却是一个能垒为+1.2 kcal/mol的非自发过程. 在StO与CuAAs初始配位后, TBAB助催化剂的Br^-靠近Com_1的C原子(StO中的α/β-C), 形成具有弱范德华相互作用的三分子复合物Com_2.

随后, Br^-通过亲核加成从背面攻击StO的α/β-C原子, StO发生开环反应, 经TS_1形成稳定的结构Com_3. 该基元反应中的过渡态TS_1对应于C−O的键断裂和C−Br键的形成. CuGly的开环能垒为+19.4 kcal/mol, 与CuAla(+21.2 kcal/mol)和CuIle(+21.3 kcal/mol)相比具有一定的能量优势, 而CuPhe的开环能垒(+28.3 kcal/mol)明显高于CuGly, 这是由于CuPhe/TBAB具有较大的空间位阻从而不利于Com7_3的形成.

接着, CO_2分子进入催化系统形成Com_4. CO_2与CuGly、CuAla、CuIle和CuPhe的配位具有较小的吸附能(分别为−8.7、−9.7、−10.5和−9.9 kcal/mol), 表明该过程的热效应较弱. 值得注意的是, 考虑了CO_2与

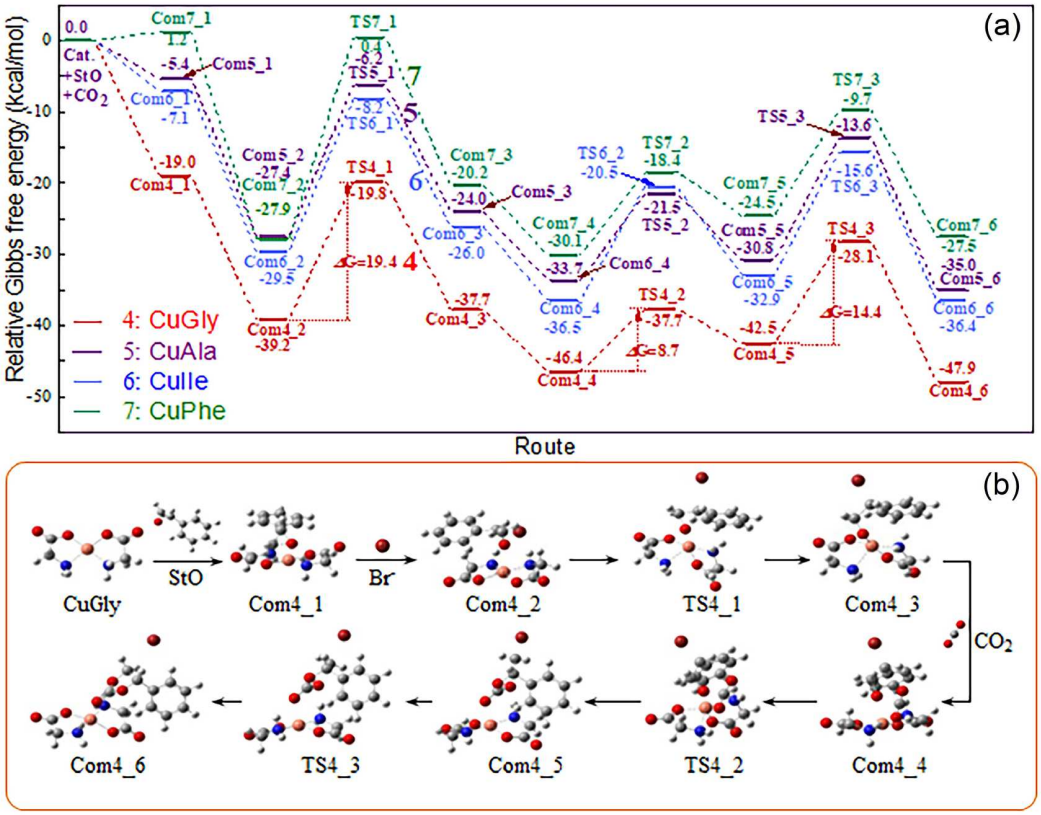

图 5 (网络版彩色)CuAAs/TBAB催化反应的吉布斯自由能分布图(a)及CuGly/TBAB催化中优化的可能中间体和TS图(b)

Figure 5 (Color online) Gibbs free energy profiles of CuAAs/TBAB catalytic reaction routes (a) and the optimized intermediates and TS of CuAAs/TBAB catalytic reaction routes (b)

Com_3潜在结合位点的各种可能性，最有利的结合位是CO_2的C原子(Lewis酸位点)以亲电加成的方式进攻已经打开的StO(强Lewis碱区)的O原子区域[51]，然后将CO_2分子插入Cu−O(StO中)键并生成中间体物种Com_5. 过渡态TS_2(TS4_2(CuGly)、TS5_2(CuAla)、TS6_2(CuIle)和TS7_2(CuPhe))的能垒分别为+8.7、+12.2、+16.0和+11.7 kcal/mol, 该过程的能垒差异主要来自于CuAAs和Br-StO配合所构建的催化平台的协同作用. 在Com_6中，碳酸酯分子经过渡态TS_3(TS4_3(CuGly)、TS5_3(CuAla)、TS6_3(CuIle)和TS7_3(CuPhe))实现闭环, 其能垒分别为+14.4、+17.2、+17.3和+14.8 kcal/mol, 该反应过程的活性差异主要来自于CuAAs活性中心区域表面静电势的影响. 反应经过渡态TS_3后形成CuAAs与环碳酸酯的配合物(Com_6), 最后经Br^-的离去和环碳酸酯的解离而完成催化循环. 综合比较四种CuAAs的DFT计算结果可知，CuGly/TBAB体系因具有更适宜的协同催化平台而呈现最佳的催化活性, DFT计算结果与实验事实是基本一致的.

2.5 CuGly与TBAX(X=Cl, Br, I)的协同催化机理

基于CuGly/TBAB优秀的协同催化效果[21,52]，对比考察了CuGly/TBAX助催化剂(X=Cl, Br, I)的催化活性, 图6为CuGly/TBAX催化体系的吉布斯自由能分布, CuGly/TBAC和CuGly/TBAI体系中可能中间体和TS的优化结构见图S5.

DFT计算结果表明，按照Cl^-(+13.6 kcal/mol) < Br^-(+19.4 kcal/mol) < I^-(+29.1 kcal/mol)的顺序, StO的开环能垒依次增加，这与卤离子亲核性相反(顺序为$Cl^->Br^->I^-$)，因为亲核性越强的助催化剂通常越容易破坏Cα/β−O键来促进StO开环，这与实验结果是一致的. 碳酸酯的闭环能垒顺序为Cl^-(+16.7 kcal/mol) > Br^-(+14.4 kcal/mol) > I^-(+13.1 kcal/mol), 这与卤离子作为离去基团离去能力的趋势一致($Cl^- < Br^- < I^-$). 由此可以推断，季铵盐卤离子的亲核性和离去能力之间的平衡决定了TBAX助催化剂的活性[53,54]. 简而言之, 亲核性好的Cl^-(TBAC)，其协同催化碳酸酯闭环的活化能最高，而对于亲核性相对较差的I^-(TBAI)，其协同催化StO开环的活化能最高. DFT 计算结果还表明，三者在CO_2插入步骤的自由能垒差别不大(均在+8.7~+10.0 kcal/mol范围内)，则其对CO_2插入步骤影响差异较小. 这是因为卤素阴离子距离CO_2插入反应位点较远，卤素阴离子对Cu-O(StO中)活性区域的EPS静电势的贡献较小. 因此，CuGly/TBAB是最有潜力的协同催化体系.

2.6 CuGly/TBAB催化体系的IGMH弱相互作用分析

IGMH分析方法[40,55~57]是基于实际电子密度的化学体系内各部分相互作用的图形表示方法. IGMH既能有效地展示系统中分子片段之间的弱相互作用，也能展现出它们之间强相互作用(化学键强度)，IGMH分析结果为进一步揭示催化剂与底物之间以多重色散相互作用(MADI)构筑的协同催化效应提供了有力证据[58]. 将催化体系中的StO(或苯乙烯碳酸酯)、Br(TBAB)、CuGly和CO_2定义为4个分子片段，确定其等面为0.004

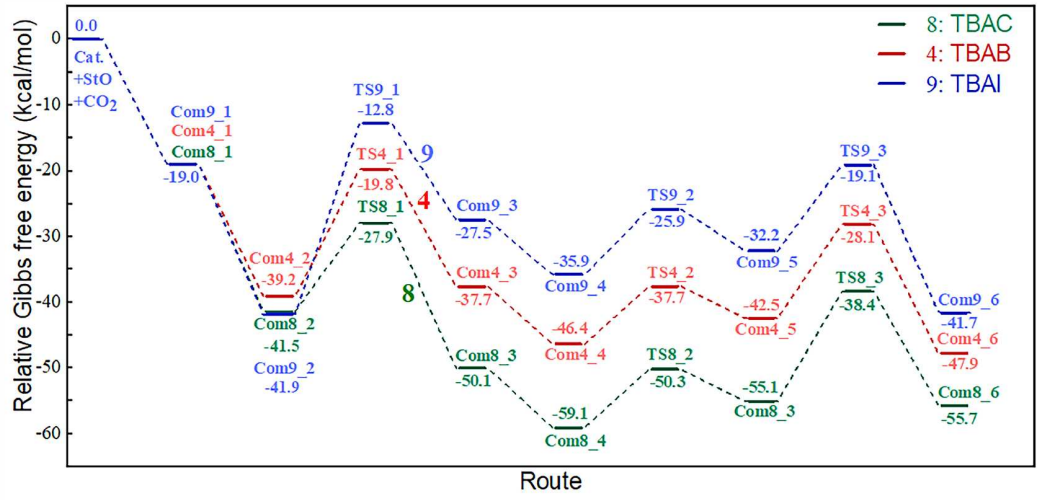

图 6 (网络版彩色)CuGly/TBAX (X=Cl, Br, I)催化反应的吉布斯自由能分布图

Figure 6 (Color online) Gibbs free energy profiles of CuGly/TBAX (X=Cl, Br, I) catalytic reaction routes

hartree, 对比分析催化体系中各分子片段之间的相互作用, 计算结果如图7所示. 蓝色的等值面代表了强而有吸引力的相互作用, 这种相互作用最常见的特征是氢键和强卤键, 绿色等值面表示弱相互作用, 分子间范德华相互作用符合这一特征, 如Br-C(Cα-StO)之间"肥厚"的等值面表明彼此之间呈现较强的配位作用. 在Br^-催化的StO开环和碳酸酯闭环过程中, 它们之间的等值面经历了一个由"薄瘦"到"肥厚"的循环过程, 说明两者之间的相互作用经历了一个由小到大再到小的循环变化. CuGly从Br^-(TBAB)的对面参与StO的开环过程, 构建了一个高电负性的Cu-O(StO的O原子)活性中心位点, CO_2以其带正电的C原子直接进攻上述活性中心, 在活性中心配体的共同作用下, 通过过渡态TS4_2, 在合适的空间位置插入到StO的C-O中, 这个过程完全受益于CuGly和Br^-的协同效应. 由此可见, CuGly和TBAB构建的协同催化网络为反应提供了一个空间定向的平台, 从而调节了催化体系中StO环开环、CO_2活化与插入、碳酸酯闭环过程中反应物种的协同作用, 为反应的顺利完成提供了合适的催化位点. 对催化体系的IGMH分析进一步表明, CuGly/TBAB之所以能够实现CO_2与StO的环加成反应, 是由于其有效协同催化作用的结果.

3 结论

CO_2与环氧化物的环加成反应是合成环碳酸酯重要的方法之一. 本工作以廉价的天然氨基酸为配体, 制备了CuAAs配合物催化剂, 应用于CO_2与StO环加成反应. TBAX为助催化剂, 环碳酸酯的收率可达71.3%~85.1%. 通过实验与DFT理论计算相结合, 研究了CuAAs和TBAX在CO_2环加成反应中的协同作用机制, 发现StO的开环过程是反应的决速步骤, CuGly和TBAB协同催化体系具有较低的过渡态能垒(+19.4 kcal/mol). 在StO开环、CO_2插入和碳酸酯闭环过程中, TBAX的协同作用主要影响StO的开环和碳酸酯的闭环过程, CuAAs配合物则主要促进CO_2的活化. 本论文构建了系列简单可行的CO_2环加成协同催化策略, 可为CO_2的捕集、储存和利用提供实验和理论支持, 为设计高效的CO_2环加成反应协同催化体系奠定了基础, 对实现涉及能源与环境的"双碳"战略目标具有一定的科学意义.

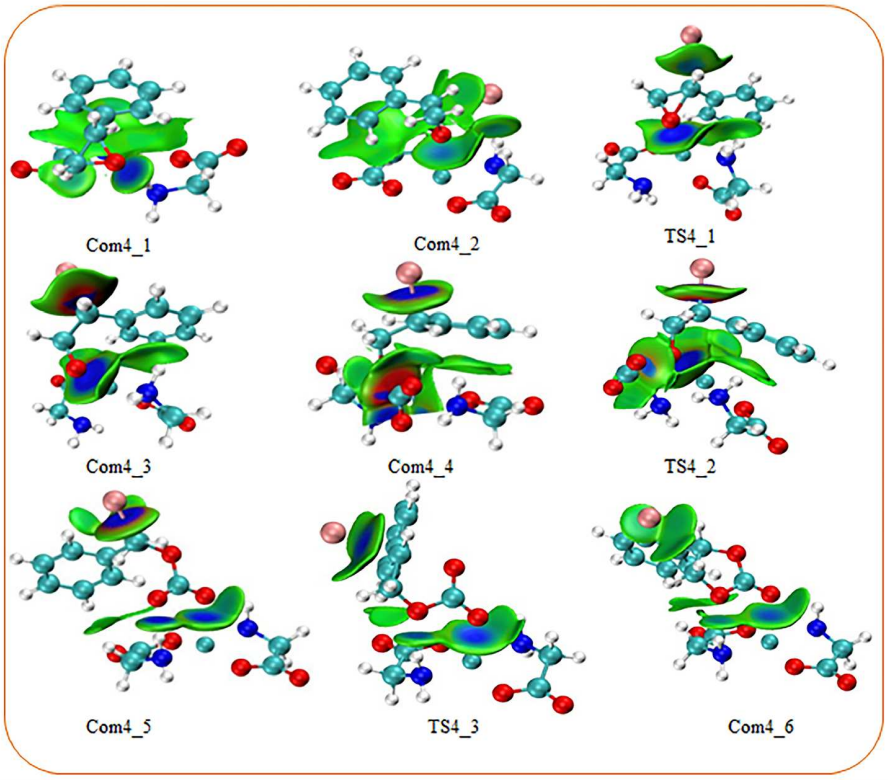

图 7 (网络版彩色)CuGly/TBAB催化体系中各分子片段间的弱相互作用图(等值面=0.004 hartree)
Figure 7 (Color online) Interaction diagram between molecular fragments in various species of CuGly/TBAB (isosurface = 0.004 hartree)

参考文献

1 Zhang Y, Jackson C, Krevor S. The feasibility of reaching gigatonne scale CO_2 storage by mid-century. Nat Commun, 2024, 15: 6913
2 Ding Z L, Zhang T. Carbon Neutrality: Logical System and Technical Requirements. Beijing: Science Press, 2022
3 He L N. Carbon dioxide chemistry: carbon capture, activation and utilization (in Chinese). Chin Sci Bull, 2021, 66: 713–715 [何良年. 二氧化碳化学: 碳捕集、活化与资源化. 科学通报, 2021, 66: 713−715]
4 Hepburn C, Adlen E, Beddington J, et al. The technological and economic prospects for CO_2 utilization and removal. Nature, 2019, 575: 87–97
5 Luo H, Ren J, Sun Y, et al. Recent advances in chemical fixation of CO_2 based on flow chemistry. Chin Chem Lett, 2023, 34: 107782
6 Zhu X, Ge T, Wu J, et al. Large-scale applications and challenges of adsorption-based carbon capture technologies (in Chinese). Chin Sci Bull, 2021, 66: 2861–2877 [朱炫灿, 葛天舒, 吴俊晔, 等. 吸附法碳捕集技术的规模化应用和挑战. 科学通报, 2021, 66: 2861−2877]
7 Ngassam Tounzoua C, Grignard B, Detrembleur C. Exovinylene cyclic carbonates: multifaceted CO_2-based building blocks for modern chemistry and polymer science. Angew Chem Int Ed, 2022, 61: e202116066
8 Zhang S, Xia Z, Zou Y, et al. Interfacial frustrated Lewis pairs of CeO_2 activate CO_2 for selective tandem transformation of olefins and CO_2 into cyclic carbonates. J Am Chem Soc, 2019, 141: 11353–11357
9 Ni H, Zhao K, Liu S, et al. Transformation of carbon dioxide in flue gas for the synthesis of formamides via Cu/In_2O_3 (in Chinese). Chin Sci Bull, 2025, 70: 1966–1976 [倪红岩, 赵康, 柳淑娟, 等. Cu/In_2O_3催化转化烟道气中二氧化碳制备甲酰胺. 科学通报, 2025, 70: 1966-1976]
10 Kim J, Kim S, Park J, et al. Covalent-frameworked 2D crown ether with chemical multifunctionality. J Am Chem Soc, 2024, 146: 4532–4541
11 Jin Y, Caner J, Nishikawa S, et al. Catalytic direct hydrocarboxylation of styrenes with CO_2 and H_2. Nat Commun, 2022, 13: 7584
12 Lyu H, Wang X, Sun W, et al. Maximizing the ionic liquid content and specific surface area in hierarchically nanoporous hypercrosslinked poly (ionic liquid)s towards the efficient conversion of CO_2 into cyclic carbonates. Green Chem, 2023, 25: 3592–3605
13 Xiao Y C, Sun S S, Zhao Y, et al. Reactive capture of CO_2 via amino acid. Nat Commun, 2024, 15: 7849
14 Zhou Y, Zhang W, Ma L, et al. Amino acid anion paired mesoporous poly(ionic liquids) as metal-/halogen-free heterogeneous catalysts for carbon dioxide fixation. ACS Sustain Chem Eng, 2019, 7: 9387–9398
15 Velisoju V K, Cerrillo J L, Ahmad R, et al. Copper nanoparticles encapsulated in zeolitic imidazolate framework-8 as a stable and selective CO_2 hydrogenation catalyst. Nat Commun, 2024, 15: 2045
16 Chen X, Song J Y, Zheng J, et al. Metal variance in multivariate metal–organic frameworks for boosting catalytic conversion of CO_2. J Am Chem Soc, 2024, 146: 19271–19278
17 Hoseini K S, Razaghi M, Nouri T, et al. Direct coupling of CO_2 with epoxides catalyzed by lanthanum(III) supported on magnetic mesoporous organosilica nanoparticles. Sci Rep, 2023, 13: 5521
18 Selden C R, Schilling K, Godfrey L, et al. Metal-binding amino acid ligands commonly found in metalloproteins differentially fractionate copper isotopes. Sci Rep, 2024, 14: 1902
19 Xu Y, Shu H, Liu J, et al. The research progress on CO_2 absorption and conversion by metal coordination-based (chelate-based) ionic liquids (in Chinese). Chin Sci Bull, 2021, 66: 728–738 [许映杰, 舒荷刚, 刘佳佳, 等. 金属配位(螯合)型离子液体在二氧化碳吸收和转化中的研究进展. 科学通报, 2021, 66: 728−738]
20 Jeong G S, Kathalikkattil A C, Babu R, et al. Cycloaddition of CO_2 with epoxides by using an amino-acid-based Cu(II)–tryptophan MOF catalyst. Chin J Catal, 2018, 39: 63–70
21 Sharifzadeh Z, Morsali A. Amine-functionalized metal-organic frameworks: from synthetic design to scrutiny in application. Coord Chem Rev, 2022, 459: 214445
22 Ran C K, Chen X W, Gui Y Y, et al. Recent advances in asymmetric synthesis with CO_2. Sci China Chem, 2020, 63: 1336–1351
23 Pal T K, De D, Bharadwaj P K. Metal–organic frameworks for the chemical fixation of CO_2 into cyclic carbonates. Coord Chem Rev, 2020, 408: 213173
24 Wang T, Ge K, Wu Y, et al. Designing moisture-swing CO_2 sorbents through anion screening of polymeric ionic liquids. Energy Fuels, 2017, 31: 11127–11133
25 Xie Y, Sun Q, Fu Y, et al. Sponge-like quaternary ammonium-based poly(ionic liquid)s for high CO_2 capture and efficient cycloaddition under mild conditions. J Mater Chem A, 2017, 5: 25594–25600
26 Yang H, Wang X, Ma Y, et al. Quaternary ammonium-based ionic liquids bearing different numbers of hydroxyl groups as highly efficient catalysts for the fixation of CO_2: a theoretical study by QM and MD. Catal Sci Technol, 2016, 6: 7773–7782
27 El-Hendawy M M, Desoky I M, Mohamed M M A. A DFT-design of single component bifunctional organocatalysts for the carbon dioxide/propylene oxide coupling reaction. Phys Chem Chem Phys, 2021, 23: 26919–26930
28 Chaban V V. Carbon dioxide chemisorption by ammonium and phosphonium ionic liquids: quantum chemistry calculations. J Phys Chem B, 2022, 126: 5497–5506

29 Liu A, Chen Y, Liu P, et al. Conversion of CO_2 to epoxides or oxazolidinones enabled by a Cu^{I} /Cu^{II}-organic framework bearing a tri-functional linker. Inorg Chem Front, 2022, 9: 4425–4432

30 Yamauchi O, Sakurai T, Nakahara A. Histidine-containing ternary amino acid-copper(II) complexes. Syntheses and properties. J Am Chem Soc, 1979, 101: 4164–4172

31 Chavez-Urias I F, López-González L E, Plascencia-Martínez D F, et al. L-Isoleucine-Schiff base copper(II) coordination polymers: crystal structure, spectroscopic, hirshfeld surface, and DFT analyses. ACS Omega, 2023, 8: 24601–24614

32 Bikas R, Soltani B, Sheykhi H, et al. Synthesis, crystal structure and magneto-structural studies of 2D copper(II) coordination polymer containing L-alanine amino acid. J Mol Structure, 2018, 1168: 195–201

33 Mao W S, Xiao Z S, Li L H, et al. Highly efficient and tunable catalytic addition of CO_2 with epoxides over 2D Co-TCPP nanosheet at ambient condition. Mol Catal, 2023, 536: 112901

34 Zhang H, Hu J, Zhao J, et al. Spectrometric measurements and DFT studies on new complex of copper (II) with 2-((E)-9-ethyl-3-(2-(6-(4-methylpyridin-2-yl)pyridin-3-yl)vinyl)-9H-carbazole. SpectroChim Acta Part A-Mol Biomol Spectr, 2016, 168: 78–85

35 Sabolović J, Gomzi V. Structure prediction of bis(amino acidato)copper(II) complexes with a new force field for molecular modeling. J Chem Theor Comput, 2009, 5: 1940–1954

36 Rulíšek L, Havlas Z. Theoretical studies of metal ion selectivity. 1. DFT calculations of interaction energies of amino acid side chains with selected transition metal ions (Co^{2+}, Ni^{2+}, Cu^{2+}, Zn^{2+}, Cd^{2+}, and Hg^{2+}). J Am Chem Soc, 2000, 122: 10428–10439

37 Berestova T V, Khursan S L, Mustafin A G. Experimental and theoretical substantiation of differences of geometric isomers of copper(II) α-amino acid chelates in ATR-FTIR spectra. SpectroChim Acta Part A-Mol Biomol Spectr, 2020, 229: 117950

38 Bahota A S, Singh K K, Yadav A, et al. Density functional theory study of Cu_6 nanoclusters as a phenylalanine detector. ACS Omega, 2024, 9: 276–282

39 Colaneri M J, Vitali J, Peisach J. Aspects of structure and bonding in copper−amino acid complexes revealed by single-crystal EPR/ENDOR spectroscopy and density functional calculations. J Phys Chem A, 2009, 113: 5700–5709

40 Shin H, Liu X, Lacelle T, et al. Mechanistic insight into bis(amino) copper formate thermochemistry for conductive molecular ink design. ACS Appl Mater Interfaces, 2020, 12: 33039–33049

41 Lu T, Chen F. Multiwfn: a multifunctional wavefunction analyzer. J Comput Chem, 2012, 33: 580–592

42 Humphrey W, Dalke A, Schulten K. VMD: visual molecular dynamics. J Mol Graphics, 1996, 14: 33–38

43 Frisch M J, Trucks G W, Schlegel H B, et al. Gaussian 09. Revision A.02. Wallingford: Gaussian Inc., 2009

44 Cui G, Wang J, Zhang S. Active chemisorption sites in functionalized ionic liquids for carbon capture. Chem Soc Rev, 2016, 45: 4307–4339

45 Zhang Y, Qiu M, Li J, et al. One-step supramolecular construction of Lewis pair poly(ionic liquids) for atmospheric CO_2 conversion to cyclic carbonates. Fuel, 2023, 332: 126191

46 Seyedhosseini B, Izadyar M, Housaindokht M R. A computational exploration of H_2S and CO_2 capture by ionic liquids based on α-amino acid anion and N_7,N_9-dimethyladeninium cation. J Phys Chem A, 2017, 121: 4352–4362

47 Maurya R C, Malik B A, Mir J M, et al. Oxidovanadium(IV) complexes involving dehydroacetic acid and β-diketones of bioinorganic and medicinal relevance: their synthesis, characterization, thermal behavior and DFT aspects. J Mol Structure, 2015, 1083: 343–356

48 Wang Y, Liu H, Shi Q, et al. Single-atom titanium on mesoporous nitrogen, oxygen-doped carbon for efficient photo-thermal catalytic CO_2 cycloaddition by a radical mechanism. Angew Chem Int Ed, 2024, 63: e202404911

49 Song B, Liang Y, Zhou Y, et al. CO_2-based stable porous metal–organic frameworks for CO_2 utilization. J Am Chem Soc, 2024, 146: 14835–14843

50 Tyagi P, Singh D, Malik N, et al. Metal catalyst for CO_2 capture and conversion into cyclic carbonate: progress and challenges. Mater Today, 2023, 65: 133–165

51 Beiragh H H, Samipourgiri M, Rashidi A, et al. Crab shell-based hierarchical micro/meso-porous carbon as an efficient nano-adsorbent for CO_2/CH_4 separation: experiments and DFT modeling. Sci Rep, 2024, 14: 18566

52 Eisenhardt K H S, Fiorentini F, Lindeboom W, et al. Quantifying CO_2 insertion equilibria for low-pressure propene oxide and carbon dioxide ring opening copolymerization catalysts. J Am Chem Soc, 2024, 146: 10451–10464

53 Zhou H, Zhang L, Wang G, et al. Fabrication of 2D metal–organic framework nanosheets with highly colloidal stability and high yield through coordination modulation. ACS Appl Mater Interfaces, 2021, 13: 39755–39762

54 Xu K, Moeljadi A M P, Mai B K, et al. How does CO_2 react with styrene oxide in Co-MOF-74 and Mg-MOF-74? Catalytic mechanisms proposed by QM/MM calculations. J Phys Chem C, 2018, 122: 503–514

55 Lu T, Chen Q. Independent gradient model based on Hirshfeld partition: a new method for visual study of interactions in chemical systems. J Comput Chem, 2022, 43: 539–555

56 Liu Z, Lu T, Chen Q. Intermolecular interaction characteristics of the all-carboatomic ring, cyclo[18]carbon: focusing on molecular adsorption and stacking. Carbon, 2021, 171: 514–523

57 Liu N, Chen F, Tao S. Hydrogen bond donors promoted organocatalyzedcycloaddition of CO_2 with epoxides (in Chinese). Chin Sci Bull, 2020, 65: 3373–3388 [刘宁, 陈飞, 陶晟. 氢键给体促进有机催化的CO_2与环氧化物的环加成反应. 科学通报, 2020, 65: 3373–3388]
58 Guan J, Luo Y, Wang Q, et al. Copper-catalyzed asymmetric hydrogenation of unsymmetrical ortho-Br substituted benzophenones. Angew Chem Int Ed Engl, 2024, 63: e202416313

补充材料

图S1 CuAAs的TEM和XPS图谱
图S2 助催化剂TBAB的用量对CO_2环加成反应的影响
图S3 CuGly/TBAB的重复利用实验结果
图S4 CuAAs/TBAB催化CO_2环加成反应中的中间体与过渡态(4~7)
图S5 CuAAs/TBAB催化CO_2环加成反应中的中间体与过渡态(8~9)

本文以上补充材料见网络版csb.scichina.com, 补充材料为作者提供的原始数据, 作者对其学术质量和内容负责.

Summary for “季铵盐离子液体对氨基酸铜催化CO_2环加成反应的协同机制”

Synergistic mechanism of quaternary ammonium salt ionic liquid in CO_2 cycloaddition reaction catalyzed by amino acid copper

Zisheng Xiao, Siyi Liu, Tuxuan Song, Dan Li, Zhili Lan, Yi Xiao*, Rong Tan* & Dulin Yin

National & Local Joint Engineering Laboratory for New Petro-chemical Materials and Fine Utilization of Resources, College of Chemistry and Chemical Engineering, Hunan Normal University, Changsha 410081, China

* Corresponding authors, E-mail: xiaoyi@hunnu.edu.cn; yiyangtanrong@126.com

CO_2 capture, storage, and utilization technologies are essential for achieving carbon peaking and neutrality targets. The efficient conversion and utilization of CO_2 as a feedstock contributes significantly to environmentally friendly and sustainable development goals. Among various CO_2 conversion strategies, the cycloaddition of epoxides with CO_2 represents a key transformation, yielding cyclic carbonates that serve as solvents, polycarbonate precursors, and fine chemicals. However, the chemical conversion of CO_2 often requires harsh reaction conditions and highly active catalysts owing to its high thermodynamic stability and kinetic inertness. Therefore, the development of catalytic systems under mild conditions is imperative. Current CO_2 cycloaddition reactions typically rely on homogeneous/heterogeneous catalysts, such as amino acid ionic liquids and MOFs. Copper amino acid complexes (CuAAs) have garnered significant attention in CO_2 cycloaddition owing to their biocompatibility and CO_2-activating ability. Furthermore, quaternary ammonium salt (TBAX) ionic liquids exhibit significant advantages in C–O bond formation owing to their distinctive physicochemical properties. Nevertheless, the catalytic systems of both CuAAs and TBAX often exhibit inadequate performance in CO_2 cycloaddition reactions. Notably, recent evidence indicates that TBAX can generate synergistic effects in catalytic systems composed of ionic liquids and metal catalysts for CO_2 cycloaddition, although the precise mechanism remains unclear. Herein, four naturally occurring amino acids, including glycine (Gly), alanine (Ala), isoleucine (Ile), and phenylalanine (Phe), were coordinated with copper nitrate. The obtained CuAA complexes (CuGly, CuAla, CuIle, and CuPhe) were characterized employing Fourier transform infrared spectroscopy, powder X-ray diffraction, and X-ray photoelectron spectroscopy. The synergistic effects of CuAAs and TBAX in the cycloaddition of CO_2 with styrene oxide (StO) under mild conditions (80°C, 1 atm CO_2) were investigated. Experimental results demonstrated cyclic carbonate yields of 71.3%–85.1% using this CuAAs/TBAX system.

Density functional theory (DFT) calculations revealed three potential non-synergistic pathways and six synergistic routes for the cycloaddition, including epoxide ring opening, CO_2 insertion, and carbonate ring closure. Surface electrostatic potential (ESP) analysis indicated that the maximum positive ESP energy for CuGly (+51.99 kcal/mol) exceeded those of other CuAAs. DFT calculations identified epoxide ring opening as the rate-limiting step for CO_2 cycloaddition. Notably, the CuGly/TBAB system exhibited the lowest transition-state barrier (+19.4 kcal/mol) compared with that of CuAla (+21.2 kcal/mol), CuIle (+21.3 kcal/mol), and CuPhe (+28.3 kcal/mol), indicating superior catalytic efficiency in the ring-opening step. In CuGly/TBAX (X = Cl, Br, I) catalytic systems, the ring-opening barriers of StO exhibited a reverse trend (Cl^-: +13.6 kcal/mol < Br^-: +19.4 kcal/mol < I^-: +29.1 kcal/mol) compared with halide nucleophilicity ($Cl^- > Br^- > I^-$). By contrast, the carbonate ring-closing barriers (Cl^-: +16.7 kcal/mol > Br^-: +14.4 kcal/mol > I^-: +13.1 kcal/mol) were consistent with halide leaving-group tendencies. These findings demonstrate that CuAAs and TBAX cooperatively promote ring-opening, CO_2 insertion, and carbonate ring-closure. TBAX primarily accelerates epoxide ring-opening and carbonate cyclization, whereas CuAAs enhance CO_2 activation.

Independent gradient model based on Hirshfeld partition analysis indicated that weak intermolecular interactions within the catalytic system, such as hydrogen bonding and electrostatic effects, are essential for the observed synergistic catalysis. The CuGly/TBAB forms a spatially oriented platform that facilitates cooperative catalysis achieved via multiple attractive dispersion interactions between the catalyst and substrates, demonstrated that weak intermolecular interactions constitute the fundamental basis for synergistic catalysis.

By combining experimental and theoretical results, this study elucidates the synergistic catalytic mechanism of CuAAs/TBAX in CO_2 cycloaddition, providing experimental and theoretical foundations for green CO_2 chemical conversion pathways. Furthermore, it offers a feasible technical solution for the resource utilization of CO_2 aligning with “dual carbon” goals.

amino-acid-Cu complexes, quaternary ammonium salt ionic liquid, CO_2 cycloaddition, synergistic catalytic reaction, DFT

doi: 10.1360/CSB-2025-0589